Fission-fragment mass distributions from strongly damped shape evolution

J. Randrup,[1] P. Möller,[2] and A. J. Sierk[2]

[1]*Nuclear Science Division, Lawrence Berkeley National Laboratory, Berkeley, California 94720, USA*
[2]*Theoretical Division, Los Alamos National Laboratory, Los Alamos, New Mexico 87545, USA*

Random walks on five-dimensional potential-energy surfaces were recently found to yield fission-fragment mass distributions that are in remarkable agreement with experimental data. Within the framework of the Smoluchowski equation of motion, which is appropriate for highly dissipative evolutions, we discuss the physical justification for that treatment and investigate the sensitivity of the resulting mass yields to a variety of model ingredients, including in particular the dimensionality and discretization of the shape space and the structure of the dissipation tensor. The mass yields are found to be relatively robust, suggesting that the simple random walk presents a useful calculational tool. Quantitatively refined results can be obtained by including physically plausible forms of the dissipation, which amounts to simulating the Brownian shape motion in an anisotropic medium.

I. INTRODUCTION

A recent study performed random walks on five-dimensional (5D) potential-energy surfaces and extracted fission-fragment mass distributions that are in remarkable agreement with experimental data [1]. The striking simplicity of the calculation, its unprecedented predictive power, and the availability of tabulated potential-energy surfaces for essentially all nuclei of potential interest [2] raise the prospect that the method may provide a quantitatively useful calculational tool for obtaining approximate fission mass yields for a large region of the nuclear chart.

However, before such applications can be made with any confidence, a number of issues need to be clarified, in particular why such a simple, and somewhat arbitrary, treatment can yield such apparently good results. Because of the potential utility of the treatment, we address these issues below.

As discussed already in the pioneering papers by Meitner and Frisch [3] and Bohr and Wheeler [4,5] in 1939, nuclear fission can be viewed qualitatively as an evolution of the nuclear shape from that of a single compound nucleus to two receding fragments. The character of the shape dynamics is still not well established but, as a step away from a purely statistical approach toward a full dynamical treatment, it is interesting to explore scenarios in which the shape evolution is strongly dissipative.

Early studies of fission dynamics with the so-called one-body dissipation suggested that the nuclear shape motion is strongly damped [6,7] and it was advocated that a reasonable starting point for determining the average evolution would be to balance the conservative force provided by the potential energy with just the friction force resulting from the dissipative coupling between the deforming nuclear surface and the nucleon gas [7,8]. A simple feature of strongly damped motion is that the inertial forces are relatively unimportant so it is less crucial to know the inertial-mass tensor for the shape motion.

The earliest numerical studies of dissipation in fission dynamics were focused on the damping effect on the mean motion only, using various physical models for dissipation, including inertial effects, and using macroscopic potentials [6,7,9,10]. Consideration of the stochastic force in fission dynamics began as early as 1940, when Kramers considered the average delay in establishing a stationary flow rate over a one-dimensional barrier, thus inferring an increase of the fission lifetime due to dissipation [11]. Further approximate treatments of the Fokker-Planck equation in one or two dimensions began around 1980 [12–16]. These calculations often retained the assumption of a constant inertia and dissipation, with very simplified potentials. About a decade later, numerical investigations of Langevin equations for dynamics including inertia, damping, and Markovian stochastic forces were begun by several groups; reviews of such work were given in Refs. [17,18]. These types of simulations continue [19–21]. They employ two or three shape degrees of freedom, macroscopic potential energies, fluid dynamic inertias, and more recent calculations usually use some form of one-body dissipation. Because of the use of macroscopic energies, they are often explicitly characterized as applying to systems with significant excitation energy.

In contrast, the present investigation focuses on systems having relatively low excitation energy, such as those produced by thermal neutrons, where it is essential to include microscopic (shell) effects in the potential energy. For 5254 even-even nuclei with $170 \leqslant A \leqslant 330$, such potential energies have been calculated with the macroscopic-microscopic method on a five-dimensional lattice of 5 315 625 shapes [2]. These potential-energy surfaces are the most comprehensive currently available and form the basis for our present studies.

II. FORMAL FRAMEWORK

We picture the nuclear fission process as an evolution of the nuclear shape from a relatively compact mononucleus to a dinuclear configuration. The nuclear shape is described by a set of parameters, $\boldsymbol{\chi} = \{\chi_i\}$, whose time development is the result of a complicated interplay between a variety of effects, as we now discuss.

Most basic, and also most easy to understand, is the potential energy associated with a given shape, $U(\boldsymbol{\chi})$, for which a number of relatively mature models have been developed. We employ potential-energy surfaces that have been calculated with the macroscopic-microscopic method in which the potential energy is the sum of shape-dependent macroscopic (liquid-drop-type) terms and a microscopic correction that reflects the structure of the single-particle levels in the effective potential associated with the specified nuclear shape [22]. The potential energy provides the driving force, $\boldsymbol{F}^{\mathrm{pot}}(\boldsymbol{\chi})$, which has the components $F_i^{\mathrm{pot}} = -\partial U/\partial \chi_i$.

The driving force seeks to change the nuclear shape and the associated matter rearrangement gives rise to a collective kinetic energy. Furthermore, the shape degrees of freedom are coupled dissipatively to the internal nuclear degrees of freedom and, as a result, the shape evolution is both damped and diffusive. The nuclear shape dynamics should therefore be treated by transport methods that allow for the stochastic elements of the dynamics. Stochastic transport approaches to nuclear dynamics have been reviewed in Refs. [17,18].

The Lagrangian associated with the shape degrees of freedom has a standard form,

$$\mathcal{L}(\dot{\boldsymbol{\chi}}, \boldsymbol{\chi}) = \tfrac{1}{2} \sum_{ij} \dot{\chi}_i \, M_{ij}(\boldsymbol{\chi}) \, \dot{\chi}_j - U(\boldsymbol{\chi}), \qquad (1)$$

and the (generalized) momentum can be obtained as $\boldsymbol{\pi} \equiv \partial \mathcal{L}/\partial \dot{\boldsymbol{\chi}}$, with the components being $\pi_i = \sum_j M_{ij}\dot{\chi}_j$. The inertial-mass tensor $\boldsymbol{M}(\boldsymbol{\chi})$ is not as well understood as the potential energy and cannot yet be calculated with comparable accuracy. In the present investigation, the inertia is ignored because it is expected to play a relatively minor role if the dissipation is strong (see below).

To a first approximation, the average effect of the coupling between the shape and the residual system is a simple friction described by a Rayleigh dissipation function,

$$\mathcal{F}(\dot{\boldsymbol{\chi}}, \boldsymbol{\chi}) = \tfrac{1}{2} \sum_{ij} \dot{\chi}_i \, \gamma_{ij}(\boldsymbol{\chi}) \, \dot{\chi}_j = \tfrac{1}{2}\dot{Q}, \qquad (2)$$

which is equal to half the average rate at which energy is being transferred to the internal degrees of freedom. The dissipation tensor $\boldsymbol{\gamma}(\boldsymbol{\chi})$ governs the associated friction force $\boldsymbol{F}^{\mathrm{fric}}(\boldsymbol{\chi})$, with $F_i^{\mathrm{fric}} = -\partial \mathcal{F}/\partial \dot{\chi}_i = -\sum_j \gamma_{ij}\dot{\chi}_j$. We shall invoke the simple *wall formula* [7] to obtain estimates of $\boldsymbol{\gamma}(\boldsymbol{\chi})$ (see Sec. III).

The average shape evolution $\bar{\boldsymbol{\chi}}(t)$ is then governed by the Lagrange-Rayleigh equation,

$$\frac{d}{dt}\bar{\boldsymbol{\pi}} = \frac{\partial \mathcal{L}}{\partial \boldsymbol{\chi}} - \frac{\partial \mathcal{F}}{\partial \dot{\boldsymbol{\chi}}}, \qquad (3)$$

where the derivatives should be evaluated along the mean trajectory. When the damping is strong, the resulting motion is slow. In that scenario, the acceleration terms as well as terms of second order in the velocities may be neglected. The corresponding creeping evolution is then determined by the demand that the friction force exactly counterbalance the driving force, i.e., $\boldsymbol{F}^{\mathrm{pot}} + \boldsymbol{F}^{\mathrm{fric}} \doteq \boldsymbol{0}$. This equation can then be solved for the average velocity $\dot{\bar{\boldsymbol{\chi}}}$, $\dot{\bar{\chi}}_i \doteq \sum_j \mu_{ij} F_j^{\mathrm{pot}}$, where the mobility tensor $\boldsymbol{\mu}$ is the inverse of the dissipation tensor $\boldsymbol{\gamma}$. Because the dissipation rate $\dot{Q}$ is always positive, the tensor $\boldsymbol{\gamma}$ is positive definite; so its inverse $\boldsymbol{\mu}$ always exists and its eigenvalues are positive.

The friction force represents the average of the interactions of the shape with the internal degrees of freedom. As is common, we shall assume that the remaining interaction is stochastic and the associated force is denoted by $\boldsymbol{F}^{\mathrm{ran}}(t)$. (Its time dependence is indicated explicitly because it is expected to vary rapidly on the time scale of the shape evolution.) By definition, it vanishes on the average, $\langle \boldsymbol{F}^{\mathrm{ran}}(t)\rangle = \boldsymbol{0}$, and we assume that its time dependence is Markovian, so $\langle F_i^{\mathrm{ran}}(t)F_j^{\mathrm{ran}}(t')\rangle = 2T\gamma_{ij}\delta(t-t')$, where $T(\boldsymbol{\chi})$ is the shape-dependent nuclear temperature (see below).

The actual shape evolution is thus both damped and diffusive and the trajectory $\boldsymbol{\chi}(t)$ is governed by the Smoluchowski equation of motion in which the driving force from the potential is counterbalanced by the full dissipative force, i.e., $\boldsymbol{F}^{\mathrm{pot}} + \boldsymbol{F}^{\mathrm{fric}} + \boldsymbol{F}^{\mathrm{ran}} \doteq \boldsymbol{0}$. This condition immediately yields the instantaneous velocity,

$$\dot{\boldsymbol{\chi}}(t) \doteq \boldsymbol{\mu} \cdot (\boldsymbol{F}^{\mathrm{pot}} + \boldsymbol{F}^{\mathrm{ran}}(t)). \qquad (4)$$

We assume that the nuclear shape evolution is described by this equation and it is thus akin to Brownian motion. The net displacement accumulated in the course of a brief time interval Δt is then

$$\delta\boldsymbol{\chi} = \int_0^{\Delta t} \dot{\boldsymbol{\chi}}(t)\, dt = \boldsymbol{\mu} \cdot \left[\boldsymbol{F}^{\mathrm{pot}}\Delta t + \int_0^{\Delta t} \boldsymbol{F}^{\mathrm{ran}}(t)\, dt \right], \quad (5)$$

where we have chosen Δt to be so small that both the driving force and the mobility tensor can be considered as constant. The first term in the above expression (5) is deterministic and represents the average displacement, corresponding to the mean trajectory provided by the Lagrange-Rayleigh equation (3), whereas the second term is stochastic and arises from the inherent thermal fluctuations that give the evolution a diffusive character.

Because of the diffusive nature of the dynamics, it is appropriate to describe the system by a probability density $P(\boldsymbol{\chi}; t)$. The average shape is then described by

$$\bar{\boldsymbol{\chi}}(t) = \int d\boldsymbol{\chi}\, \boldsymbol{\chi}\, P(\boldsymbol{\chi}; t), \qquad (6)$$

while the fluctuations around the average are characterized by the correlation tensor $\boldsymbol{\sigma}(t)$ having the elements

$$\sigma_{ij}(t) = \int d\boldsymbol{\chi}\, (\chi_i - \bar{\chi}_i(t))(\chi_j - \bar{\chi}_j(t))\, P(\boldsymbol{\chi}; t). \qquad (7)$$

When starting from a given shape specified by $\boldsymbol{\chi}_0$, we have $P(\boldsymbol{\chi}; t=0) = \delta(\boldsymbol{\chi} - \boldsymbol{\chi}_0)$ and the distribution then shifts and broadens in the course of time. In the Fokker-Planck approximation, this evolution is described by

$$\frac{\partial}{\partial t} P = \left[-\sum_i \frac{\partial}{\partial \chi_i}\mathcal{V}_i + \sum_{ij} \frac{\partial}{\partial \chi_i}\frac{\partial}{\partial \chi_j}\mathcal{D}_{ij} \right] P(\boldsymbol{\chi}; t), \quad (8)$$

where $\mathcal{V}(\boldsymbol{\chi})$ is the drift coefficient (vector) and $\mathcal{D}(\boldsymbol{\chi})$ is the diffusion coefficient (tensor). These transport coefficients are simply related to the early evolution of an initially narrowly defined distribution, namely,

$$\frac{d}{dt}\bar{\boldsymbol{\chi}} = \mathcal{V} = \boldsymbol{\mu} \cdot \boldsymbol{F}^{\mathrm{pot}}, \qquad \frac{d}{dt}\boldsymbol{\sigma} = 2\mathcal{D} = 2\boldsymbol{\mu}T. \qquad (9)$$

The drift rate $\dot{\chi}$ follows immediately from (5) and the diffusion rate $\dot{\sigma}$ is also readily obtained because the covariance matrix for the changes in χ is given by

$$\langle \delta\boldsymbol{\chi}\,\delta\boldsymbol{\chi}\rangle = \int_0^{\Delta t}\int_0^{\Delta t} \langle \dot{\boldsymbol{\chi}}(t)\,\dot{\boldsymbol{\chi}}(t')\rangle\, dt\, dt' \qquad (10)$$

$$= \int_0^{\Delta t}\int_0^{\Delta t} \boldsymbol{\mu}\cdot\langle \boldsymbol{F}^{\mathrm{ran}}(t)\,\boldsymbol{F}^{\mathrm{ran}}(t')\rangle\cdot\boldsymbol{\mu}\, dt\, dt' \qquad (11)$$

$$= \int_0^{\Delta t}\int_0^{\Delta t} 2T\boldsymbol{\gamma}\,\delta(t-t')\, dt\, dt' = 2T\boldsymbol{\mu}\Delta t. \quad (12)$$

We note that $\mathcal{V}T = \mathcal{D}\cdot\boldsymbol{F}^{\mathrm{pot}}$ in accordance with the fluctuation-dissipation (Einstein) relation [23].

The nuclear shape, being a macroscopic entity, is treated as a classical variable. But it is in contact with the microscopic degrees of freedom which are quantal in nature. Therefore, one should generally use the appropriate quantal form of the Einstein relation. However, in the present case, because we are considering the strongly damped limit, the surface motion is very slow and the relation reverts to its simple classical form [see Eq. (9)]. For the specific dissipative mechanism considered here, i.e., the one-body wall dissipation (see Sec. III), the energy dissipated in an elementary process (the reflection of a nucleon off the moving surface) is given by $\omega \approx -mV_F\dot{n}$, where m is the nucleon mass and V_F is its Fermi speed, while $\dot{n}$ is the surface velocity. The temperature T in the Einstein relation should then be replaced by $T^* = \frac{1}{2}\omega\coth(\omega/2T)$. But $\dot{n}$ is very small in the considered overdamped limit, $|\omega|\ll T$, so $T^*\approx T$ and the classical form is appropriate. This is in contrast to the situation in damped nuclear collisions where the relative nuclear speed is not negligible and the operating one-body window dissipation is characterized by the quantal form of the Einstein relation, as is directly reflected in the strong dependence of the variance of the fragment mass distribution on the dissipated energy [24,25].

A. Direct simulation

One way to proceed is to solve the Fokker-Planck transport equation (8), which is a partial differential equation for a time-dependent function of N variables (in our case, $N = 5$; see below). This is a formidable task and we instead perform direct Monte Carlo simulations of the Smoluchowski equation of motion (4) to generate suitably large samples of individual stochastic shape evolutions.

For this purpose, it is convenient to write the mobility tensor explicitly in terms of its eigenvectors, $\{\tilde{\boldsymbol{\chi}}^{(n)}\}$, normalized such that $\tilde{\boldsymbol{\chi}}^{(n)}\cdot\tilde{\boldsymbol{\chi}}^{(n)}$ is the eigenvalue μ_n (which is always positive, as explained above),

$$\mu_{ij} = \sum_n \tilde{\chi}_i^{(n)}\tilde{\chi}_j^{(n)}. \qquad (13)$$

Assuming now that the current shape is characterized by the value χ, we wish to propagate the shape forward to a slightly later time, $t + \Delta t$. The average shape change is readily obtained from Eq. (5) as $\delta\overline{\boldsymbol{\chi}} = \boldsymbol{\mu}\cdot\boldsymbol{F}^{\mathrm{pot}}\Delta t$. The random contribution to the shape change is most easily sampled in the eigenframe of the mobility tensor because the increments

in each principal direction may be sampled separately. By invoking the eigenrepresentation of $\boldsymbol{\mu}$ (13), we may then obtain the total increment in χ accumulated in the course of the small time interval Δt,

$$\delta\boldsymbol{\chi} = \sum_n \tilde{\boldsymbol{\chi}}^{(n)}[\Delta t\,\tilde{\boldsymbol{\chi}}^{(n)}\cdot\boldsymbol{F}^{\mathrm{pot}} + \sqrt{2T\Delta t}\,\xi_n], \qquad (14)$$

where $\{\xi_n\}$ are random numbers sampled from a standard normal distribution having zero mean and unit variance. This propagation procedure is easily implemented, once the mobility tensor $\boldsymbol{\mu}$ has been diagonalized. The average of the accumulated change is then

$$\delta\bar{\chi}_i = \Delta t\sum_n \tilde{\chi}_i^{(n)}\,\tilde{\boldsymbol{\chi}}^{(n)}\cdot\boldsymbol{F}^{\mathrm{pot}}, \qquad (15)$$

because $\langle\xi_n\rangle = 0$, and the accumulated correlation σ_{ij} becomes

$$\sigma_{ij} = 2T\Delta t\sum_n \tilde{\chi}_i^{(n)}\,\tilde{\chi}_j^{(n)}, \qquad (16)$$

because $\langle\xi_n\xi_{n'}\rangle = \delta_{nn'}$. Both are proportional to Δt.

It is an important feature of the propagation scheme (14) that when the time interval Δt is sufficiently small, the generated ensemble of dynamical histories remains unaffected by a subdivision of the time interval, so the numerical solution of the transport problem is robust. To see this, imagine that the time interval used in Eq. (14) is subdivided into a number of shorter intervals, $\{\Delta t^{(m)}\}$, with $\sum_m \Delta t^{(m)} = \Delta t$. If $\boldsymbol{\mu}$, $\boldsymbol{F}$, and T remain unchanged during Δt, the resulting combined change in χ becomes $\delta\boldsymbol{\chi} = \sum_m \delta\boldsymbol{\chi}^{(m)}$, with

$$\delta\boldsymbol{\chi}^{(m)} = \sum_n \tilde{\boldsymbol{\chi}}^{(n)}\big[\Delta t^{(m)}\,\tilde{\boldsymbol{\chi}}^{(n)}\cdot\boldsymbol{F}^{\mathrm{pot}} + \sqrt{2T\Delta t^{(m)}}\,\xi_n^{(m)}\big]. \quad (17)$$

Recalling that $\langle\xi_n^{(m)}\rangle$ vanishes, we see that the combined average change remains the same as before,

$$\sum_m \langle\delta\boldsymbol{\chi}^{(m)}\rangle = \sum_n \tilde{\boldsymbol{\chi}}^{(n)}\left(\sum_m \Delta t^{(m)}\right)\tilde{\boldsymbol{\chi}}^{(n)}\cdot\boldsymbol{F}^{\mathrm{pot}}, \quad (18)$$

as does the accumulated covariance σ_{ij},

$$\left\langle\left(\sum_m \delta\chi_i^{(m)}\right)\left(\sum_m \delta\chi_j^{(m)}\right)\right\rangle = 2T\left(\sum_m \Delta t^{(m)}\right)\sum_n \tilde{\chi}_i^{(n)}\tilde{\chi}_j^{(n)}, \qquad (19)$$

because $\langle\xi_n^{(m)}\xi_{n'}^{(m')}\rangle = \delta_{mm'}\delta_{nn'}$. Thus the diffusion process is robust under changes in the employed time interval Δt, as it should be. Of course, this invariance pertains to the *distribution* of dynamical histories, $P(\chi;t)$, whereas any individual trajectory does change when Δt is changed.

A related invariance holds when the overall magnitude of the dissipation tensor $\boldsymbol{\gamma}$ is changed: If the elements $\gamma_{ij}(\chi)$ are all increased by the common factor $N(\chi)$, then the local time evolution proceeds at a rate that is $N(\chi)$ times slower, but the resulting distribution of shape trajectories, $P(\chi;t)$, remains the same. This convenient feature allows us to arbitrarily rescale the friction locally to facilitate the numerical treatment, because we are not here interested in the actual time evolution but merely in the final distribution of mass divisions. Such local rescaling of the dissipation tensor is equivalent to adjusting

the local clock rate, which will obviously not affect the outcome of the process but merely change how much time is spent at various locations. For convenience, we shall therefore assume that the eigenvalues $\gamma_n(\chi)$ are one on average, for each particular shape χ.

B. Discrete random walk

It is instructive to consider the simple situation when the mobility tensor is aligned with the lattice, i.e., μ is diagonal, $\mu_{ij} = \mu_i \delta_{ij}$. The transport process then reduces to a standard random walk, i.e., Eq. (14) reduces to

$$\delta\chi_i = \mu_i F_i \Delta t + \sqrt{2T\mu_i \Delta t}\, \xi_i. \quad (20)$$

If the potential energy U is known for any value of the shape parameter χ, then the local force F can be obtained as the corresponding gradient, $F_i^{\text{pot}} = -\partial U/\partial\chi_i$, and the transport process (20) can be readily simulated to yield an ensemble of evolutions. Because each increment $\delta\chi_i$ is a real number (i.e., not necessarily an integer), each evolution is represented by a sequence of shapes whose coordinates $\{\chi_i\}$ may take on any fractional value within the considered parameter domain.

However, the potential energy employed [2] is available only on a discrete lattice whose 5 315 625 sites are labeled by the integers $\{I, J, K, L, M\}$, corresponding to integer values of the shape coordinates, $\{\chi_1, \ldots, \chi_5\}$. By performing a pentalinear interpolation (see Appendix A), we may obtain an approximate representation of the potential energy for arbitrary (fractional) values of the shape coordinates, $U(\chi)$, and the above continuous transport process (20) may then be simulated.

A simpler but approximate treatment of the above continuous transport problem consists of performing a random walk on the discrete lattice, i.e., the shape parameters $\{\chi_i\}$ take on only integer values. This can be conveniently accomplished by means of the standard Metropolis sampling procedure (see below), as was originally done in Ref. [1]. The quality of this approximation depends on the lattice spacing, and if the spacing is reduced, then the discrete random walk becomes a better approximation to the continuous transport process.

To understand how the continuous random walk (20) can be approximated by a Metropolis procedure, we first note that when the mobility tensor is diagonal, each lattice direction i is an eigendirection and can, therefore, be sampled independently. In the discrete treatment, the step size in the direction i is fixed by the lattice spacing Δ_i, and we need to know the probabilities for taking a forward or backward step during a brief time interval Δt, $P_\pm^{(i)} = \nu_\pm^{(i)} \Delta t$. The associated Fokker-Planck transport coefficients, which express the rate at which the mean location changes and half the rate at which the variance in the location grows, are therefore given by

$$\mathcal{V}_i = (\nu_+^{(i)} - \nu_-^{(i)})\Delta_i = \mu_i F_i, \quad (21)$$

$$\mathcal{D}_i = \tfrac{1}{2}(\nu_+^{(i)} + \nu_-^{(i)})\Delta_i^2 = \mu_i T, \quad (22)$$

where F_i is the force in the lattice direction i, and $\mu_i = 1/\gamma_i$ is the mobility in that direction; they are independent of the lattice spacing Δ_i. These relations can be readily solved for

the rates

$$\nu_\pm^{(i)} = \frac{\mu_i}{\Delta_i^2}\left[T \pm \frac{1}{2}F_i \Delta_i\right] \approx \frac{\mu_i}{\Delta_i^2}\left[T \mp \frac{1}{2}\Delta U_i\right], \quad (23)$$

where $\Delta U_i \equiv -F_i \Delta_i$ is the change in the potential associated with an increase of χ_i by Δ_i. It then follows that $P_+^{(i)}/P_-^{(i)} \approx \exp(-\Delta U_i/T)$, which is precisely what characterizes the Metropolis procedure, as we now show.

In the Metropolis procedure [26], a proposed step is always accepted if the associated energy change ΔU is negative, whereas it is accepted only with the probability $\exp(-\Delta U/T)$ otherwise. The probabilities for accepting the reverse step are then $\exp(\Delta U/T)$ or unity, respectively. So the ratio between the forward and backward acceptance probabilities is $P_+/P_- = \exp(-\Delta U/T)$. Thus a continuous random walk of the type (20) can be treated approximately by means of a discrete random walk based on the Metropolis procedure.

The treatment reported in Ref. [1] employed such a discrete random walk on the 5D lattice of potential energies. A bias potential of the form $V_{\text{bias}}(Q_2) = V_0 Q_0^2/Q_2^2$ was added to disfavor compact shapes and thus help to guide the walk toward the scission region, thereby speeding up the calculation; the strength used was checked to be sufficiently small so that no further reduction would affect the mass yields. Thus the only physical parameter was the critical neck radius c_0 at which it was assumed that no further change in mass asymmetry would occur; typically, the calculated mass yields were relatively insensitive to c_0 in the range of 2–3 fm, and $c_0 = 2.5$ fm was adopted as the standard value in Ref. [1].

We are now in a position to ascertain the inaccuracies that are inherent in such an approach due to the specific lattice employed in Ref. [2]. We first examine the effect of the finite magnitude of the lattice spacing by comparing the results of the Metropolis walk with those of the corresponding continuous process. This is illustrated in Fig. 1 for two typical cases (the others considered show comparable effects). The continuous process and its discrete approximation tend to yield rather similar results for the fragment mass distribution. But there are some noticeable differences in the region of the asymmetric peak for the thorium isotopes considered. Such discrepancies suggest that the results are quite sensitive to the underlying potential energy surface in that particular region of the shape space (cf. the effect of modifying the Wigner term discussed in Sec. IV C), which is a feature that might help to achieve a better understanding of the potential energy.

Second, we address the important role played by the relative size of the site spacings in the different lattice directions. The Metropolis walks carried out in Ref. [1] treated all the five lattice directions equally, which amounts to implicitly assuming that the underlying mobility tensor is isotropic, i.e., the mobilities are the same in all of the lattice directions, $\mu \sim I$. Each lattice direction has then an even chance for being considered as a candidate for the next Metropolis step. However, as the above analysis brings out, a change in the lattice spacing in one direction modifies the effective mobility in that particular direction: with an increased density of lattice sites, it takes a larger number of elementary Metropolis steps to go a given distance. Therefore, if the density of lattice sites is increased by a factor of N in the direction i,
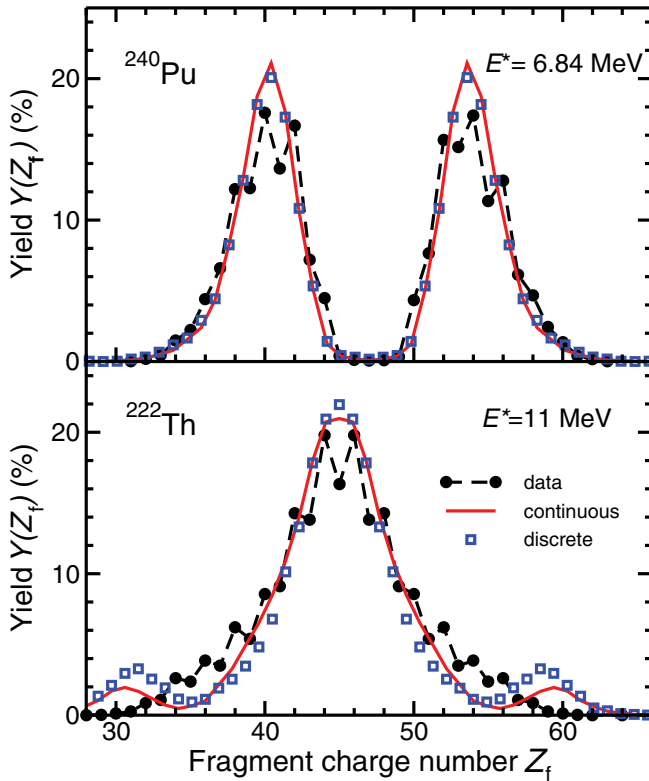
FIG. 1. (Color online) The effect of the discretization of the shape space on the calculated fragment charge distribution is illustrated by comparing the results of the Metropolis walk introduced in Ref. [1] with those of the corresponding continuous process; the experimental data [27,28] are also shown. Throughout, as in Ref. [1], the calculated mass yields $Y(A_f)$ have been transformed to charge yields by a simple scaling, $Y(Z_f) = (A_0/Z_0)Y(A_f)$, where Z_0 and A_0 are the charge and mass numbers of the fissioning nucleus. The odd-even staggering seen in the data is due to pairing and this effect is not present in the potential-energy surfaces because existing pairing models treat the fissioning nucleus as a single system, even near scission.

then the corresponding mobility coefficient is decreased by the factor N^2, $\mu_i \rightarrow \mu_i/N^2$. Conversely, to ensure that the evolution of the transport process remains unaffected by the increased density of lattice sites, the likelihood that the affected direction is being considered as a candidate for the next step must be increased by that factor. For example, if the density of lattice sites in a particular direction is doubled, $N = 2$, then the likelihood for considering that direction should be increased from $\frac{1}{5}$ to $2^2/(4+4) = \frac{1}{2}$ to achieve the same evolution.

These features are illustrated in Fig. 2 for the same two cases that were shown in Fig. 1. We consider the effect of changing the lattice spacing in the I direction, which corresponds to the overall elongation as quantified by the quadrupole moment Q_2. When the lattice spacing in the I direction is decreased by a factor of three and the Metropolis walk is repeated with no other change, then the resulting fragment mass distribution is affected quantitatively, becoming noticeably narrower. However, as suggested by the analysis above, when the corresponding mobility is also increased by a factor of nine (by favoring the consideration of the I direction
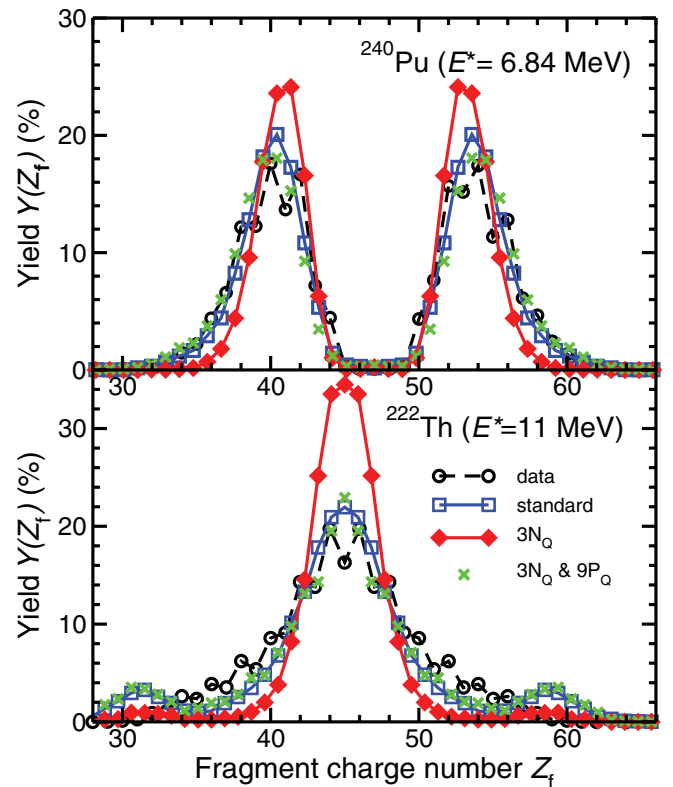
FIG. 2. (Color online) The effect of changing the lattice spacing for the Metropolis walk: The standard lattice [2] is modified in the Q_2 direction by introducing two additional lattice sites between the original lattice sites, thus tripling the density of lattice sites in that direction; subsequently, the likelihood for considering the Q_2 direction as a candidate for the next step is enhanced by a factor of nine (solid curve), which is seen to compensate exactly for the reduced lattice spacing. Also shown are the experimental data [27,28].

correspondingly), the mass distribution reverts to its original form.

The relative lattice spacings are thus intimately related to the anisotropy of the effective mobility tensor. This basic feature makes the Metropolis walks performed in Ref. [1] seem somewhat arbitrary, because a different choice of lattice spacing, without any compensating change in the mobility coefficient, would generally lead to a different final result. It is therefore important to employ a mobility tensor based on a physically plausible form of the dissipation and to investigate the sensitivity of the calculated mass distributions to that specific structure. We now turn to this central issue.

III. INCLUSION OF DISSIPATION

As discussed above, the simple random walk introduced in Ref. [1] is most easily justified if the dissipation tensor is isotropic in the employed lattice variables. Since such an idealized scenario is not likely to be realistic, we wish to study the effect of using a more plausible dissipation tensor, which is generally anisotropic and has a structure that varies from one shape to another.

The potential energy of deformation, $U(\chi)$, was calculated [2] on a lattice of shapes introduced by Nix [29,30]. As described in Appendix B, each shape is composed of three smoothly joined quadratic surfaces. These 3QS shapes are characterized by the parameters $q = \{q_\mu\}$. While these are, in principle, known functions of the lattice shape variables $\chi = \{\chi_i\}$, they are readily available only at the discrete lattice sites $\chi = (I, J, K, L, M)$.

The dissipation tensor can be determined from the rate of energy dissipation $\dot{Q}$, which is a positive definite quadratic form in the shape velocities,

$$\dot{Q} = \sum_{ij} \dot{\chi}_i \, \gamma_{ij}(\chi) \, \dot{\chi}_j = \sum_{\mu\nu} \dot{q}_\mu g_{\mu\nu}(q) \dot{q}_\nu. \quad (24)$$

The first form expresses $\dot{Q}$ in terms of the lattice variables $\{\chi_i\}$, while the second form uses the 3QS parameters $\{q_\mu\}$ so $g_{\mu\nu}(q)$ is the friction tensor with respect to these variables (see Appendix B). Once $g_{\mu\nu}(q)$ has been calculated (see below), we may obtain the required dissipation tensor $\gamma(\chi)$ by the appropriate transformation,

$$\gamma_{ij}(\chi) = \sum_{\mu\nu} \frac{\partial q_\mu}{\partial \chi_i} g_{\mu\nu}(q) \frac{\partial q_\nu}{\partial \chi_j}. \quad (25)$$

We wish to determine $\gamma(\chi)$ at the various lattice sites, at which the parameters $\{\chi_i\}$ have integer values and we approximate the derivatives $\partial q_\nu / \partial \chi_n$ in terms of differences between the values of q_ν at the neighboring sites. Although this is a relatively rough approximation because the dependence of q on χ is generally not linear, it will suffice for our present explorative purposes.

In order to calculate $g_{\mu\nu}(q)$, we thus need to know the dissipation rate $\dot{Q}(q, \dot{q})$. For that we employ the "wall formula" for the one-body dissipation mechanism [7]. The underlying mechanism is the reflection of individual nucleons off of the moving surface, which generates a dissipative force that is rather strong due to the nucleonic Fermi motion. Because the individual nucleons reach the moving surface at random times, and from random directions, the associated force on the surface is stochastic, in accordance with the fluctuation-dissipation theorem [23]. While this idealization may not give a quantitative account of the actual dissipation rate in a real fissioning nucleus, it does serve well as a means to provide us with a mobility tensor that has a quasirealistic structure.

In its simplest form, the one-body dissipation rate in a deforming nucleus is given by the simple wall formula, $\dot{Q} = m\rho_0\bar{v} \oint \dot{n}(a)^2 d^2a$, where m, ρ_0, and $\bar{v}$ are the nucleonic mass, density, and mean speed in the interior, respectively, while $\dot{n}(a)$ is the normal surface velocity at the location a [7,31]. It is elementary to show [6] that the elements of the associated dissipation tensor are given by

$$g_{\mu\nu} = \frac{\pi}{2}\rho_0\bar{v} \int \frac{\partial\rho^2(z)}{\partial q_\mu} \frac{\partial\rho^2(z)}{\partial q_\nu} \left[\rho^2 + \frac{1}{4}\left(\frac{\partial\rho^2}{\partial z}\right)^2\right]^{-\frac{1}{2}} dz, \quad (26)$$

where $\rho(z; q)$ is the transverse extension of the nucleus at the position z along the symmetry axis, for the specified values of the 3QS parameters q. The required quantities, namely,

$\rho^2(z)$ and its derivatives with respect to both z and the shape variables $\{q_\nu\}$, can be expressed analytically for the 3QS shape family [29] and so it is possible to calculate the elements of g for each specified shape.

However, as explained in Appendix B, certain elements of the dissipation tensor g may occasionally tend to zero (this happens when one of the three quadratic surfaces covers a negligible z interval so that this shrinking section ceases to contribute to the dissipation). Of course, the corresponding derivatives $\partial q_\mu / \partial \chi_i$ diverge at the same time so the resulting elements of γ remain well behaved. But, because it is impractical, for the time being, to calculate those derivatives with high accuracy, the calculation of γ is correspondingly inaccurate, with some eigenvalues occasionally becoming unrealistically small.

Fortunately, our main purpose is merely to study the sensitivity of the calculated fragment mass distributions to the structure of the dissipation tensor, and we therefore perform the following isotropization procedure. If γ is the original tensor, calculated as described above but renormalized so that its five eigenvalues $\{\gamma_n\}$ are one on average, i.e., $\sum_n \gamma_n = 5$, then we define a more isotropic tensor $\tilde{\gamma}$ by modifying the eigenvalues,

$$\tilde{\gamma}_n^{(f)} \equiv \frac{\gamma_n + f}{1 + f}, \quad (27)$$

where the isotropization coefficient f is a positive number. We see that the original friction tensor is recovered when f tends to zero, while it approaches isotropy when f grows large. The corresponding modified mobility tensor $\tilde{\mu}(f)$ is then the inverse of $\tilde{\gamma}(f)$.

The sensitivity of the calculated charge yields to the degree of structure in the mobility tensor is illustrated in Figs. 3 and 4 for the cases presented in Ref. [1]. In addition to the experimental data, which are shown for reference, each plot shows the result of three different mobility scenarios: the idealized scenario (labeled $f \gg 1$) where the mobility tensor is isotropic, an intermediate scenario ($f = 1$) in which the dissipation tensor is the average of the one calculated with the wall formula as described above and the corresponding directional average, and a more structured scenario ($f = 0.2$) in which the isotropic admixture is only 20 %.

For the three neutron-induced cases, ^{239}Pu(n,f) and ^{235,233}U(n,f), the change in $Y(Z_f)$ is very small as one form of the mobility tensor is replaced by another, with the most noticeable change being a slight narrowing of the asymmetric peaks for ^{233}U(n,f). The photon-induced reactions, which are all calculated for $E^* = 11$ MeV, display a somewhat larger sensitivity. Generally, as the idealized isotropic mobility tensor grows more anisotropic, there is a tendency for the symmetric yield component to become more prominent, but the quantitative effect is relatively modest. It is particularly noteworthy that the evolution from a symmetric yield for ^{222}Th to a mixed but predominantly asymmetric yield for ^{228}Th remains present in all the scenarios. When comparing with these data, it should be kept in mind that they represent a range of excitations ($E^* \approx 8$–14 MeV) and also are contaminated by second- and third-chance fission.
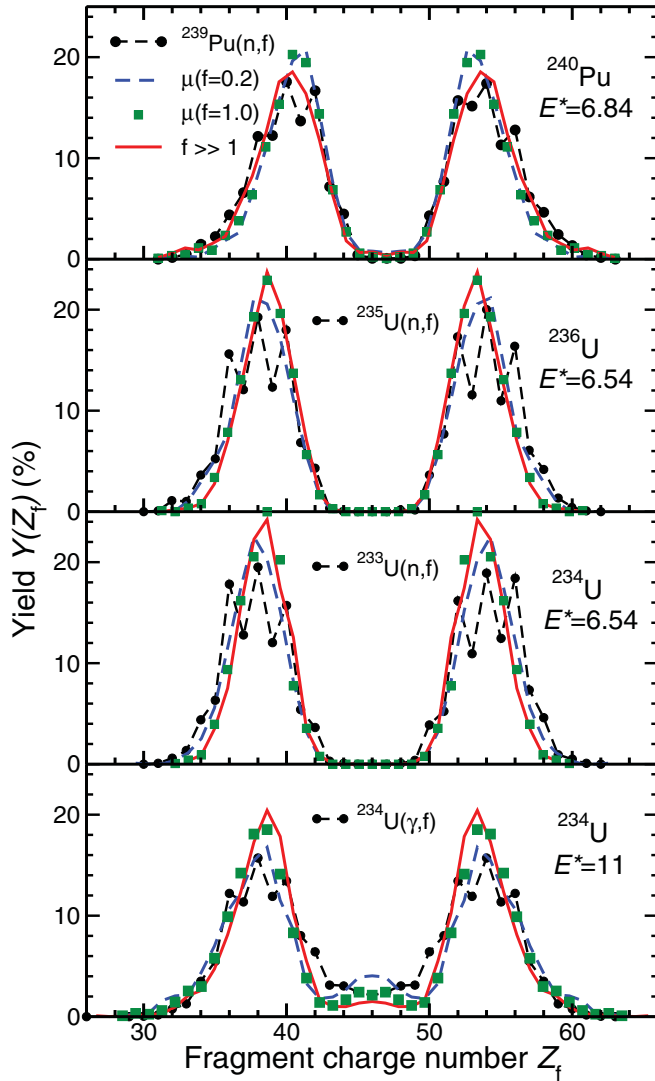
FIG. 3. (Color online) The charge yields for neutron-induced fission of ^{240}Pu and ^{236,234}U calculated with increasingly isotropic mobility tensors, as obtained by using Eq. (27) with $f = 0.2, 1, \infty$ (the latter is fully isotropic and has been indicated as $f \gg 1$), together with the experimental data [27,35]. Those in the top three panels are for (n$_{th}$,f) reactions [27], while the data in the bottom panel is for (γ,f) reactions leading to $E^* \approx 8$–14 MeV; they include contamination from multichance fission [28].
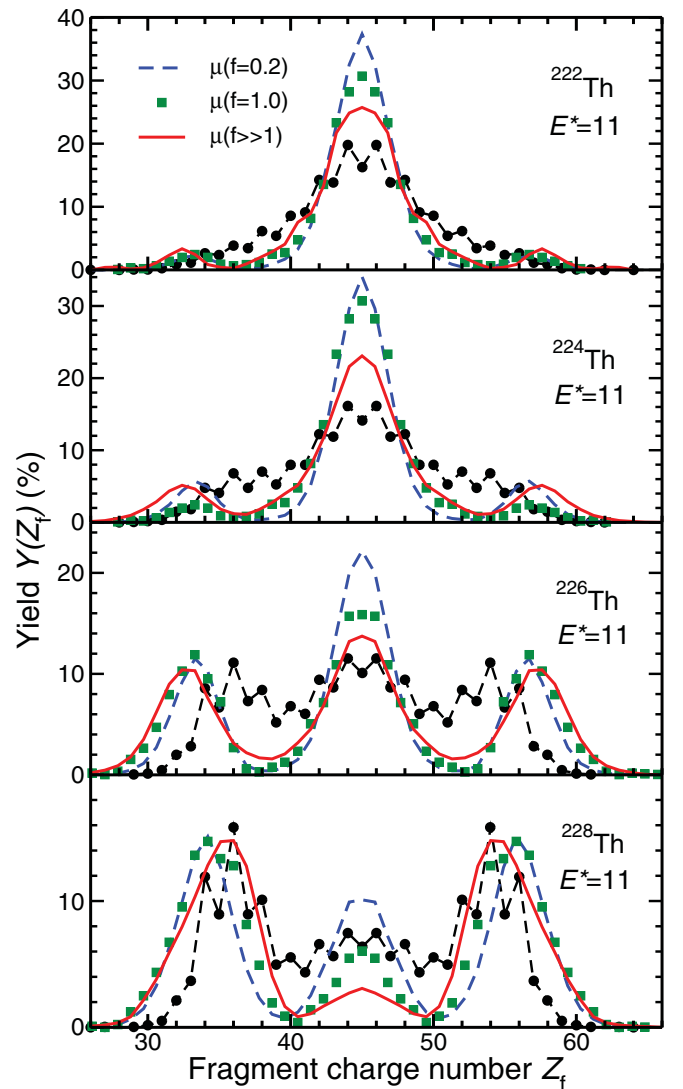

FIG. 4. (Color online) The charge yield for thorium isotopes calculated with increasingly isotropic mobility tensors, as obtained by using Eq. (27) with $f = 0.2, 1, \infty$ (the latter being fully isotropic), together with the experimental data obtained with (γ,f) reactions leading to $E^* \approx 8$–14 MeV; they include contamination from multichance fission [28].

IV. DISCUSSION

We now discuss a number of interesting aspects that can be elucidated with the present treatment.

The choice of shape degrees of freedom made in Ref. [2], and of the specific 5D shape lattice used for the calculations of the potential energy, was guided in large part by physical intuition (using the somewhat vague but reasonable criterion that the typical energy change between neighboring sites should be of comparable magnitude). Our present studies suggest that this lattice of nuclear shapes was indeed well chosen, because the simple Metropolis walks provide mass yields that are changed only moderately when a more refined treatment is made. Because the actual mobility tensor is not

yet well known, it would seem prudent to employ a range of mobility scenarios. The spread among the results might then be taken as a rough indication of the uncertainty in the prediction.

Furthermore, on the basis of our studies, it appears that the Metropolis walk, which is significantly faster than the Smoluchowski simulation (by one to two orders of magnitude), offers a very quick and easy means for obtaining practically useful fission-fragment mass distributions.

A. Shape family

We start by illustrating the importance of employing a shape family that has a sufficient degree of flexibility. For that purpose, we construct three-dimensional potential-energy surfaces by minimizing the full five-dimensional 3QS surfaces
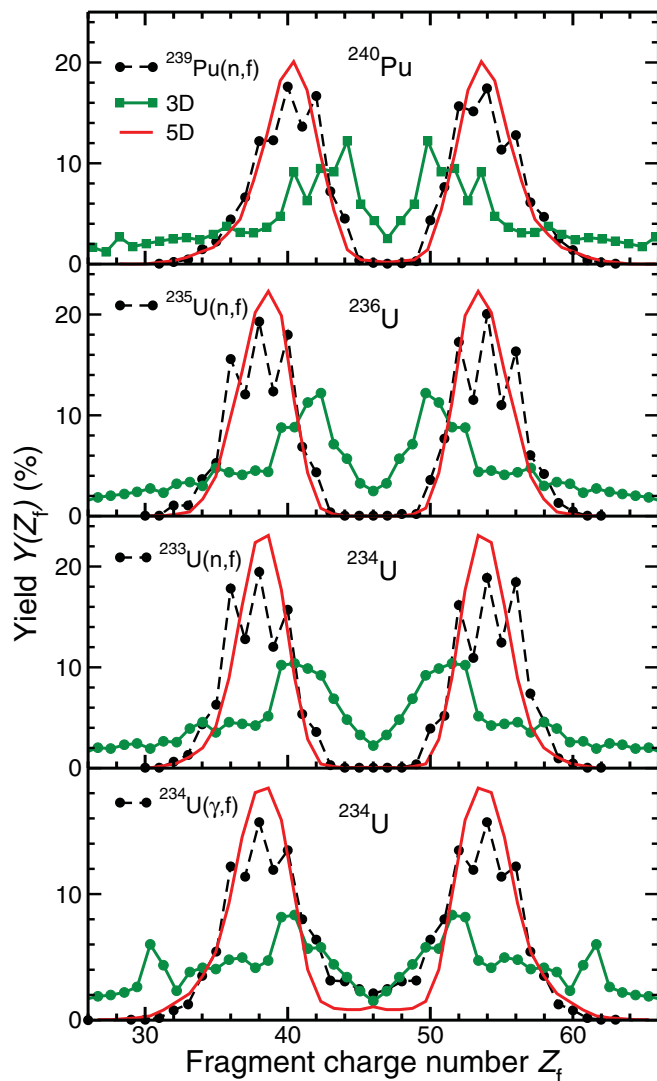
FIG. 5. (Color online) Charge yields resulting from Metropolis walks on the 5D potential-energy surfaces associated with the 3QS shape family, together with the corresponding results obtained with 3D surfaces generated by minimizing the 5D surfaces with respect to the individual fragment deformations, ϵ_{f1} and ϵ_{f2}. Also shown are the experimental data [27,28].

FIG. 6. (Color online) Similar to Fig. 5, but for fission of the isotopes ^{222,224,226,228}Th; the data are from Ref. [28].

with respect to the deformations of the two spheroids, ϵ_{f1} and ϵ_{f2} (corresponding to the lattice indices K and L). Thus the shapes in the lower-dimensional space are characterized by only their overall elongation (represented by the lattice index I), their constriction (represented by the lattice index J), and the degree of reflection asymmetry (represented by the lattice index M).

Figures 5 and 6 show the resulting charge distributions for the cases presented in Ref. [1], together with the experimental data and our standard results based on the full 5D 3QS shape family. We see that although the 3D calculations occasionally reproduce the qualitative appearance of $Y(Z_f)$ reasonably well, the reproduction of the experimental data is generally far inferior to the results obtained with the 5D shape family.
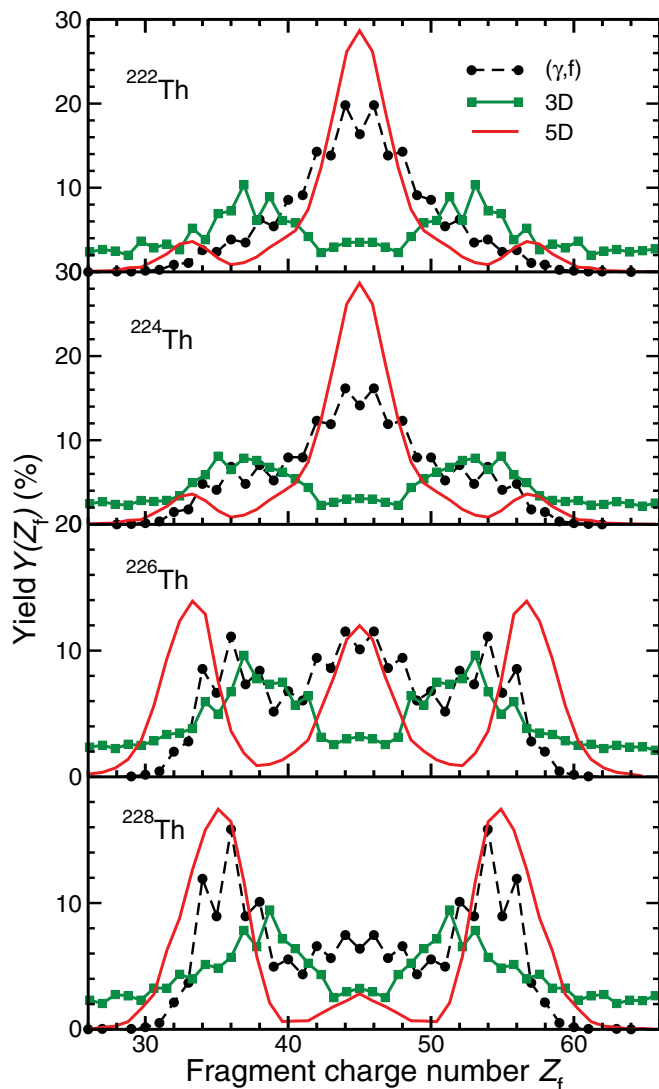
These examples demonstrate that it is important to employ a sufficiently rich family of shapes when seeking to describe the shape evolution during nuclear fission. To obtain a reasonably flexible family of shapes, at least five shape degrees of freedom appear to be required, namely, overall elongation, constriction, reflection asymmetry, and deformations of the individual prefragments.

B. Saddle shape

Because our calculational method emulates the actual equilibration process, it is possible to gain insight into the shape evolution during fission. A particularly instructive case is presented by ^{222}Th: Our calculations yield a symmetric mass distribution, in agreement with the experimental data, even though they are based on a potential-energy surface whose fission saddle point corresponds to a nuclear shape that is reflection asymmetric.
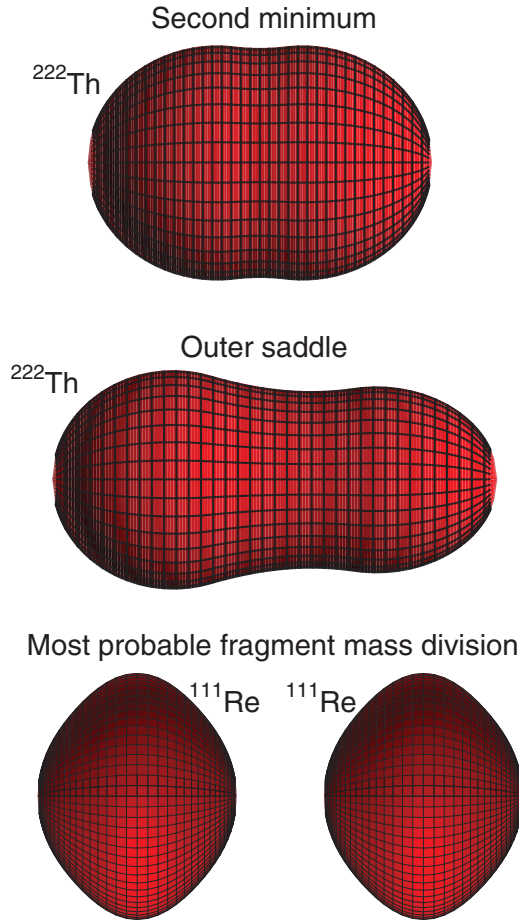
FIG. 7. (Color online) Three shapes relevant for fission of ^{222}Th: the outer potential-energy minimum (which is reflection symmetric) where the fission isomeric state resides (top), the outer saddle which is asymmetric (middle), and the most probable fragment division which is symmetric (bottom).

The most relevant shapes are shown in Fig. 7. As the shape evolves from that of the ground state, it tends to pass nearby the second (isomeric) minimum and the nucleus will typically remain trapped in that minimum for quite some time before escaping, either back to the ground-state region or toward scission. (For that reason, we usually start our calculations at the second minimum, which reduces the required computational effort very significantly; we have of course checked that this does not alter the results.) As the figure shows, the outer minimum of ^{222}Th is reflection symmetric, while the outer saddle lies in a region of significant asymmetry. Nevertheless, the shapes evolve in such a manner that the final fragment mass distribution is centered around symmetry.

More detailed insight into this evolution can be obtained by considering the charge-asymmetry distribution at specified values of the lattice index I, which is a measure of the overall quadrupole moment of the fissioning shape, $P(Z_f; I)$. This conditional distribution is shown in Fig. 8 for increasing elongations, starting at the value associated with the second saddle point, $I_{\text{saddle}} = 20$. Because it is energetically favorable for the system to traverse the barrier with an asymmetry close to that of the saddle shape, $P(Z_f; I_{\text{saddle}})$ is concentrated around
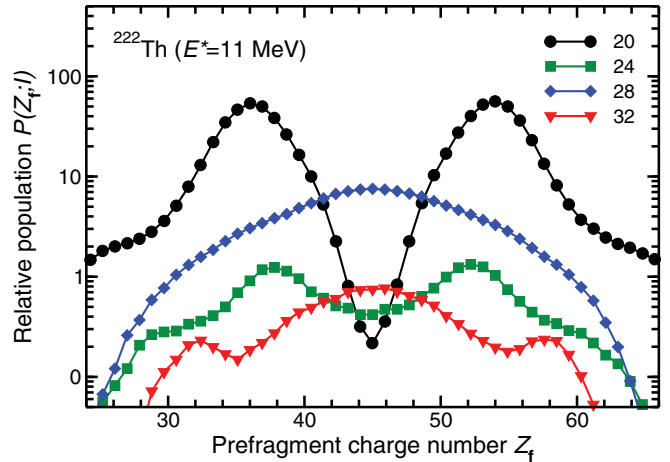

FIG. 8. (Color online) The evolution of the mass-asymmetry distribution from the region of the second saddle ($I = 20$) toward scission is illustrated by the charge distribution $P(Z_f; I)$ for increasing values of I (the lattice index giving the quadrupole moment Q_2 of the nuclear shape), as obtained for an ensemble of 10 000 Metropolis walks.

that asymmetry. However, beyond the saddle, the preferred asymmetry tends to become smaller ($I = 24$) and the asymmetry eventually becomes peaked at symmetry ($I = 28$). As the shape evolves further toward scission ($I = 32$), $P(Z_f; I)$ develops a minor asymmetric component that presumably reflects the detailed (and possibly inaccurate) structure of the potential-energy surface in the scission region (see the discussion of the Wigner term in Sec. IV C).

This result invalidates the commonly made assumption (see, e.g., Refs. [32–35]) that the character of the mass distribution, whether symmetric or asymmetric, is determined by the character of the saddle shape. In contrast, analyses of the type illustrated in Fig. 8 suggest that the structure of the potential-energy landscape in the entire region between the isomeric minimum and scission plays a role in determining the fragment mass distribution. Obviously, any plausible model of the mass yields must take this into account.

C. Wigner term

The generality of our treatment makes it possible to exploit the remaining differences between calculated results and experimental data to gain novel insight into aspects of the fission process that would not otherwise be readily accessible. As an example, we consider the shape dependence of the Wigner term in the macroscopic nuclear energy [36–41].

As mentioned above, the potential energies of Ref. [22] were calculated as the sum of a macroscopic term and a microscopic (shell) correction, both being shape dependent. The macroscopic nuclear energy contains the so-called Wigner term proportional to $|N - Z|$. Its presence is clearly visible in the systematics of nuclear masses, which exhibit a V shape near isosymmetry, but its microscopic origin is still not well understood, so it is normally modeled as a phenomenological macroscopic term. In commonly employed models for nuclear masses [42,43], the Wigner term is usually introduced without

a shape dependence. However, such an ansatz presents a significant (but often ignored) problem in fission where a single nucleus is transformed into two separate nuclei, with each having its own Wigner term. (It is evident from the phenomenological form of the term [38,39] that each fragment must give a Wigner contribution similar to that of the original nucleus.) Thus the Wigner term must double in magnitude during the evolution from a single compound system to two separated fragments, so, consequently, it must depend on the nuclear shape.

The calculations of fission barriers in, for example, Refs. [2,36,38] have since 1989 employed a postulated shape dependence that relates the increase of the Wigner term to the decrease in the amount of communication between the two fragments due to the shrinking of the neck. The resulting Wigner term changes gradually as the nuclear shape evolves and affects the potential-energy landscape correspondingly (an illustrative figure was given in Ref. [36]). However, it may be argued that the change in the character of the fissioning system from mononuclear to dinuclear occurs more abruptly than implied by the currently prescribed shape dependence. To elucidate the importance of the shape dependence of the Wigner term, we have considered an alternate form in which the term is kept constant up to the scission configuration, i.e., until the neck radius has shrunk below the specified critical value c_0.

In Fig. 9, we illustrate how such a modification of the calculated potential-energy surface affects the calculated charge distribution of ^{226}Th, for which the impact is particularly noticeable. There are two significant differences between the results of the two sets of calculations. One is a change in the relative importance of symmetric and asymmetric fission, with the constant Wigner term leading to more asymmetric yield. The other is a shift in the location of the asymmetric yield peaks, from being several units on the outside of the observed values toward a better agreement with the data. Both effects depend significantly on the structure of the mobility tensor and could, in principle, be of help in discriminating between different models of the dissipation.

D. Level density

The microscopic part of the potential energy, $\delta U_{sh}(\chi)$, is due to the deformation-dependent variations in the single-particle level densities in the effective field of the fissioning nucleus. This structure also affects the dependence of the nuclear temperature T on the excitation energy E^*. Because a change of the local temperature affects the local diffusion rate but not the drift rate, a change in $T(E^*; \chi)$ may influence the evolution of the shape distribution $P(\chi)$.

In order to explore the importance of this effect, we replace the standard Fermi-gas level-density parameter $\tilde{a}_A \equiv A/e_0$ in the formula $E^* = a_A T^2$ by a "shell-corrected" generalization suggested by Ignatyuk [44],

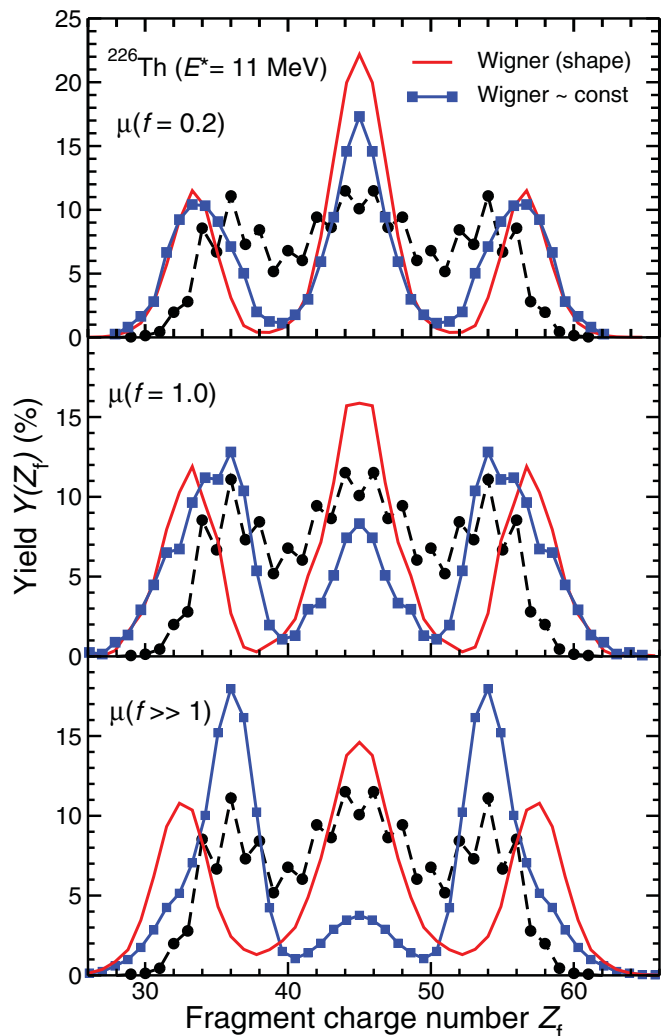$$a_A(E^*; \chi) = \tilde{a}_A \left[1 + (1 - e^{-E^*/E_{damp}}) \frac{\delta U_{sh}(\chi)}{E^*} \right], \quad (28)$$

FIG. 9. (Color online) The sensitivity of the charge yields to the shape dependence of the Wigner term is illustrated for ^{226}Th, using either the standard potential-energy surface [2], in which the Wigner term changes gradually as the shape evolves, or a modified energy surface obtained with a Wigner term that remains constant until scission occurs; the three panels show results calculated with increasingly isotropic mobility tensors as obtained by using Eq. (27) with $f = 0.2, 1, \infty$; the experimental data are also shown [28].

where E_{damp} characterizes the gradual dissolution of the shell effects as the excitation energy is increased. We shall use $e_0 = 8$ MeV and $E_{damp} = 18.5$ MeV. At low excitation, $E^* \to 0$, a_A tends to $\tilde{a}[1 + \delta U_{sh}/E_{damp}]$, while it approaches $\tilde{a}_A$ monotonically as E^* is increased (when $E^* \gg E_{damp}$, the exponential is close to zero and also $\delta U_{sh}/E^* < E_{damp}/E^* \ll 1$, since $|\delta U_{sh}| < E_{damp}$).

We have examined the effect of replacing the macroscopic formula $a_A = A/e_0$ by the above microscopic expression (28). On the whole, the calculated mass yields are remarkably unaffected by this change, probably because each random walk visits quite a large number of lattice sites, so the shell effet, which tends to fluctuate, largely averages out. The most noticeable effect occurs for the ^{234}U(γ,f) reaction, where the use of the microscopic expression leads to more
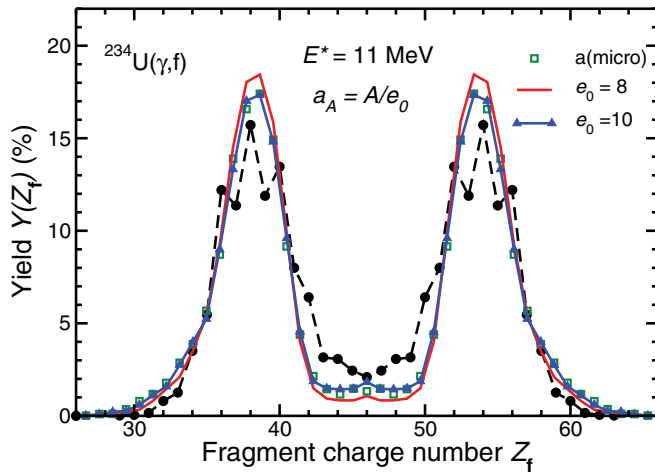
FIG. 10. (Color online) The charge yield for the ^{234}U(γ,f) reaction extracted from Metropolis walks using either the macroscopic expression for the level density, $a_A = \tilde{a}_A \equiv A/e_0$, with the standard value $e_0 = 8$ MeV and also $e_0 = 10$ MeV, or the microscopic expression (28); the experimental data are included [28].

yield in the symmetric region (where our standard calculation underpredicts the yield). This case is shown in Fig. 10, where we have also included the result of using the macroscopic formula with a larger value of e_0. Due to the relation $E^* = a_A T^2$, this change causes the local temperature to increase and, as a result, the symmetric yield is increased. As it turns out, the effect of making this increase in e_0 in the macroscopic formula is practically identical to the effect of replacing a_{macro} by a_{micro}.

We wish to point out that our present studies do not consider the effect of pairing, which may be included in a simple approximate manner by backshifting the excitation energy $E^*(\chi)$ by the pairing gap $\Delta(\chi)$ when calculating the local temperature $T(\chi)$. Such an undertaking would require knowledge of the shape-dependent pairing gap, $\Delta(\chi)$. While this quantity was of course calculated at each lattice site when the potential-energy surfaces were generated [2], it was not tabulated separately, so it is not presently available. We must therefore leave this interesting issue for future study.

E. Scission model

As already recognized in the very earliest discussions of fission theory [4,5], induced fission involves, as an intermediate stage, the formation of a compound nucleus in which the excitation energy is distributed among the various degrees of freedom in a statistical manner. However, the compound equilibrium is established only among those relatively compact shapes that are situated inside of the fission barrier, and the ensemble experiences a continual leakage as some nuclei accidentally acquire a shape far enough beyond the saddle point that they then undergo an irreversible evolution toward scission. (Elementary phase-space estimates of the leakage rate form the basis for the familiar transition-state theory of fission.) Thus the resulting fission-fragment mass distribution bears no particular relationship to the distribution of the asymmetric modes of the compound-nuclear shapes.

Furthermore, because of the nonequilibrium nature of the post-barrier evolution, there is no reason to expect that the resulting mass distribution should have a statistical form. Nevertheless, a variety of statistical scission models have been studied. Indeed, models based on such considerations were among the earliest developed [45,46] and, for each specific case, the details can often be adjusted to yield reasonable agreement with observed mass distributions. We wish to illustrate the importance of the prescission shape evolution by comparing our transport results with what a purely statistical population of the scission shapes would yield.

The quality of scission model results relies on the specific definition of the scission configurations (in our present 5D shape space, these generally form a four-dimensional hypersurface), and they tend to be rather sensitive to the parameters involved. Furthermore, such a scission hypersurface may contain some configurations that are energetically favorable but not dynamically reachable due to the presence of intermediate ridges in the potential-energy landscape; purely statistical considerations might then be qualitatively wrong. Such is presumably the case, for example, in the recently reported fission of ^{180}Hg for which symmetric splits are strongly favored by the energetics in the exit channel (and were thus widely expected), but are most likely prevented dynamically by the presence of a potential-energy ridge so that the fragment mass distribution becomes asymmetric [47].

We wish to here bring out the contrast between the considerable sensitivity of such scission-model results and the remarkable robustness of the transport results when the definition of the scission criterion is modified. For this purpose, we define a four-dimensional scission hypersurface as consisting of those shapes $\{\tilde{\chi}\}$ for which the neck radius equals a specified value, $c(\tilde{\chi}) = c_{\mathrm{sc}}$, and we then assume that these scission configurations are populated in proportion to their statistical weight, $W(\tilde{\chi}) \sim \exp[-U(\tilde{\chi})/T(\tilde{\chi})]$. As in the transport calculations, we use the shape-dependent temperature, which ensures that the statistical weight drops rapidly to zero at the boundary of the energetically accessible region of shapes, namely, those for which $U(\chi) - U_{\mathrm{gs}} \lesssim E^*$.

For four representative cases, Fig. 11 shows the results of such scission-model calculations obtained for $c_{\mathrm{sc}} = 2.5, 2.0, 1.5$ fm. In all cases, as c_{sc} is decreased through this range, the character of the fragment mass distribution changes qualitatively, from symmetric to asymmetric; the same is true for the cases not shown. (We note that the particular value $c_{\mathrm{sc}} = 2.0$ fm happens to yield a quite reasonable reproduction of the various data sets, but the large sensitivity of $P(A_f)$ to c_{sc} suggests that no significance should be ascribed to this.)

For comparison, Fig. 12 shows the corresponding results obtained with the simple Metropolis walk introduced in Ref. [1], for the same values for the critical neck radius c_0. The extracted fragment mass distributions are remarkably robust against the changes in c_0. These results demonstrate that it is not primarily the energetics in the scission region that determines the mass split, but rather the broader potential-energy landscape encountered by the shape during its prescission evolution.
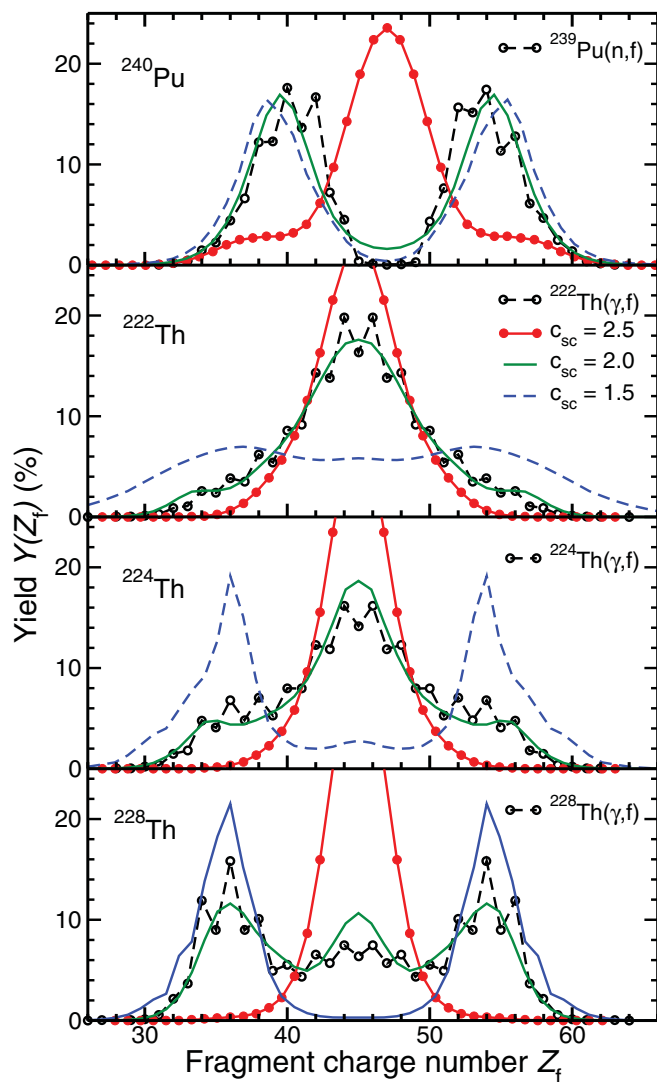
FIG. 11. (Color online) Results of our scission model (see text) for ^{240}Pu and ^{222,224,228}Th for the scission neck radii $c_{sc} = 2.5, 2.0, 1.5$ fm, together with the corresponding experimental data [27,28].
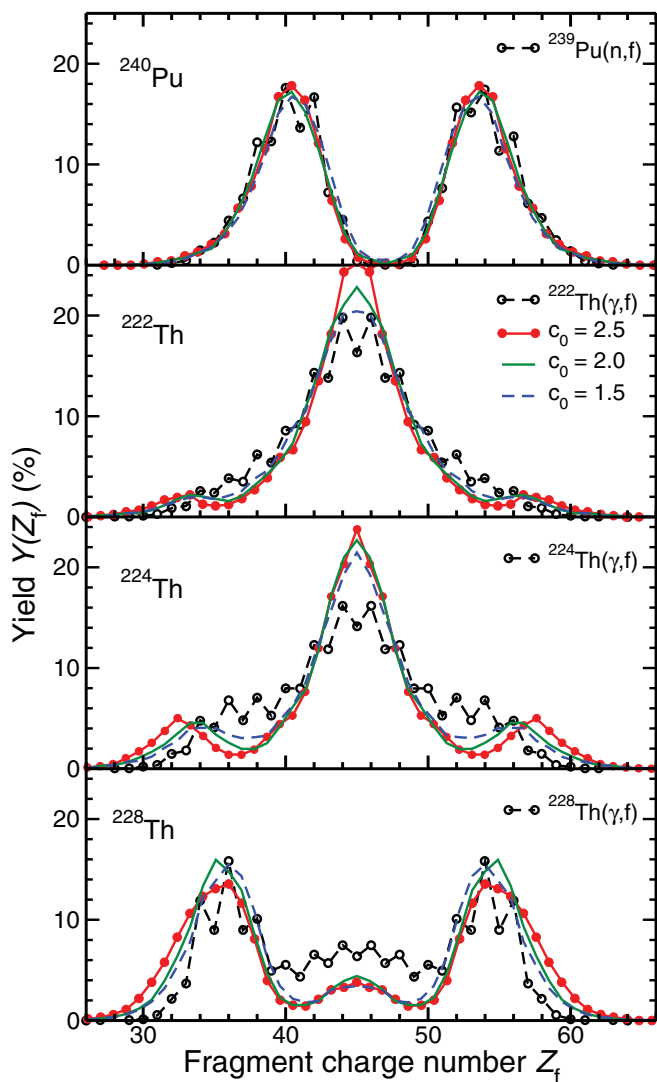
FIG. 12. (Color online) Results of the Metropolis walk [1] for the cases shown in Fig. 11, obtained with the same values of the critical neck radius c_0, together with the corresponding experimental data [27,28].

When comparing Figs. 11 and 12, it is important to appreciate the different meanings of c_0 and c_{sc}. The former is that value of the neck radius at which the transport calculation is terminated; since the mass asymmetry cannot change very rapidly when the neck is so small, the extracted mass distribution is not very sensitive to the specific value used (and the employed values are not indicative of where the system actually scissions, but rather of where the mass asymmetry is effectively frozen in). By contrast, c_{sc} is that value of the neck radius for which the statistical weights are calculated; as demonstrated, the relative values of these weights are rather sensitive to the specified value of c_{sc}.

V. CONCLUDING REMARKS

Generally, calculations of the type discussed here pertain to the idealized limit of strongly damped motion where the

inertia plays no role. The evolution of the nuclear shape is then akin to Brownian motion. Whether in fact the shape evolution during fission has such a character is still an open question, but we believe that this simple limit provides a useful reference scenario.

In a first exploration of this physical picture, it was recently shown that simple random walks on five-dimensional potential-energy surfaces lead to remarkably good agreement with experimental data on fission-fragment mass distributions [1]. We have examined this method in depth, studying the importance of a number of effects that could be expected to influence the results.

First we generalized the discrete random walk on the fixed lattice sites where the potential energy is available to a continuous diffusion process, thus enabling an assessment of the importance of the finite lattice spacing. We found that there is typically little difference between the results of the two

treatments, although we observed some deviations in certain limited regions.

Such a simple random walk, whether discrete or continuous, is physically reasonable only if the dissipation tensor happens to be isotropic in the particular shape variables employed, which is generally not expected to be the case. This important feature was illustrated by studying the effect of inserting additional sites between the standard lattice sites, which reduces the mobility in the affected direction.

The main objective of the present study is therefore to elucidate how the results of the idealized treatment may change when a more realistic dissipation tensor is employed. For this purpose, we adopted the dissipation tensor suggested by the simple one-body dissipation wall formula and introduced an isotropization procedure, which allowed us to examine a continuum of scenarios ranging from perfect isotropy (corresponding to the idealized random walks discussed above) to the relatively large degree of anisotropy displayed by the calculated friction tensors. Generally, we found that the resulting fragment mass distributions are rather insensitive to the degree of anisotropy, except, in certain cases only, for rather extreme anisotropies that are probably unrealistic and may arise from certain numerical problems.

We then examined a number of additional relevant aspects. First we demonstrated the importance of using a sufficiently rich family of shapes by comparing results based on the full 5D potential-energy surfaces with analogous calculations in a reduced 3D deformation space obtained by constrained minimization. The importance of using sufficiently flexible shapes was borne out in particular by the isotope ^{222}Th whose mass yield is symmetric even though the outer saddle shape is asymmetric.

As an example of the potential of the present method for elucidating novel aspects of nuclear properties, we examined the sensitivity of the calculated mass distribution to the character of the deformation dependence of the Wigner term in the macroscopic energy functional. Specifically, it was demonstrated for ^{226}Th that when the previously employed, rather gradual shape dependence is replaced by a more abrupt transition from the mononucleus to the dinucleus, the symmetric component of $Y(Z_f)$ is reduced and its asymmetric peaks move toward better agreement with the experimental data.

We also examined the effect of taking account of the deformation-dependent bunchings in the single-particle level densities which affect the energy dependence of the temperature for a given shape and thus the local diffusion rate relative to the drift. The calculated mass yields are relatively unaffected by this refinement, except for a favorable shift in the amount of nearly symmetric mass splits, but it should be kept in mind that the effect of the (presently unavailable) shape-dependent paring gap is still left for future study.

Finally, the importance of the prefission shape evolution was brought out by comparisons of the robust transport results with the parameter-sensitive mass distributions arising from a statistical population of the scission configurations.

For some of the cases considered here, most notably ^{239}Pu(n, f), the calculations reproduce the experimentally observed yields very well and are rather robust with respect to model variations, such as changes in the mobility tensor. Hence, for the comparisons with data to be informative, it appears to be important to examine also cases that exhibit larger sensitivity, such as the thorium isotopes.

The formal framework for the present treatment is considerably simpler than that used in a conventional Langevin-type dynamical treatment. Accordingly, the information that can be extracted is correspondingly reduced. The key assumption of strong dissipation allows us to neglect the inertial masses and this in turn reduces the equation of motion from second to first order in time. The resulting transport equation pertains to the limit of creeping motion and thus provides only the path of the fissioning nucleus in the shape space, rather than its full temporal evolution. While this limited information suffices for the extraction of the fragment masses, it is unsuitable for obtaining kinetic energies.

In conclusion, our studies suggest that the simple Metropolis walk [1] on the previously calculated potential-energy lattice [2] indeed presents a useful calculational tool for obtaining the approximate form of fission-fragment mass distributions for a large range of nuclei. For more accurate results, it is necessary to invoke also the dissipative features of the shape evolution as represented by the shape-dependent mobility tensor. The shape evolution then resembles Brownian motion in an anisotropic (and nonuniform) medium. However, because the dissipation mechanism is not yet as well understood as the potential energy, we propose to make a series of calculations with mobility tensors that display different degrees of anisotropy and then use the ensuing spread in the results as an indication of the uncertainty of the predicted mass yield. The results obtained in this manner are often remarkably robust. Consequently, the method may be of practical use for calculating fission-fragment mass distributions for any of the thousands of nuclei for which the required 5D potential-energy surface is already available.

APPENDIX A: LATTICE INTERPOLATION

The nuclear shapes are characterized by the five shape parameters $\{\chi_n\} = (\chi_1, \chi_2, \chi_3, \chi_4, \chi_5)$, which are collectively denoted by χ. But the potential energy of deformation, $U(\chi)$, is known only on a five-dimensional Cartesian lattice on which the shape parameters take on the integer values $X =$

$\{X_n\} = (I, J, K, L, M)$, whose ranges are given in Ref. [2]. (We use X to denote a capital χ.) We describe here how the potential energy for arbitrary χ values can be obtained by pentalinear interpolation, i.e., an interpolation scheme that yields a function $U(\{\chi_n\})$ that is linear in each of the five variables χ_n inside each elementary hypercube. [The resulting function is identical to the Taylor expansion around the "lower-left" hypercube corner, $X = (I^-, J^-, K^-, L^-, M^-)$, keeping only terms of first order in each variable and approximating all derivatives by the corresponding central differences.]

We assume that the given shape parameter χ lies within the domain covered by the lattice and start by identifying the surrounding elementary hypercube. Its 32 corners are given by the indices $(I^\pm, J^\pm, K^\pm, L^\pm, M^\pm)$, where $X_n^- = [\chi_n]$ (i.e., the integer part of χ_n) and $X_n^+ = X_n^- + 1$, so $X_n^- \leqslant \chi_n < X_n^+$ for $n = 1, \ldots, 5$. In a single dimension, the interpolated value would be

$$U(\chi) = U(X^-)(X^+ - \chi) + U(X^+)(\chi - X^-), \quad \text{(A1)}$$

so we may readily generalize to five dimensions,

$$\begin{aligned} U(\chi) = \sum_{ijklm} ijklm \, U(I^{-i}, J^{-j}, K^{-k}, L^{-l}, M^{-m}) \\ \times (I^i - \chi_1)(J^j - \chi_2)(K^k - \chi_3)(L^l - \chi_4)(M^m - \chi_5), \end{aligned}$$
$$\text{(A2)}$$

where the summation indices each take on the values ∓ 1. It is easy to verify that this is indeed correct: Within the local hypercube (within which χ is located), the above expression is linear in each of the five χ variables and it yields the correct matching, because when χ coincides with a lattice site, $\chi = X = (I, J, K, L, M)$, then $I^- = I, \cdots, M^- = M$, so $X_n^- - \chi_n = 0$ and $X_n^+ - \chi_n = 1$, so only the term with $i = +1, \ldots, m = +1$ contributes, yielding $U(\chi) = U(I, J, K, L, M)$.

The driving force $\boldsymbol{F} = -\nabla U(\chi)$ can be obtained by taking the derivative of the above expression (A2). Thus,

$$\begin{aligned} F_1(\chi) = -\sum_{ijklm} ijklm \, U(I^{-i}, J^{-j}, K^{-k}, L^{-l}, M^{-m}) \\ \times (J^j - \chi_2)(K^k - \chi_3)(L^l - \chi_4)(M^m - \chi_5), \quad \text{(A3)} \end{aligned}$$

and analogously for the other four directions. Thus, within the local hypercube, the force component F_n does not depend on

χ_n, as is consistent with the fact that the potential is locally linear in χ_n.

A similar scheme is used to calculate other quantities for arbitrary shapes, such as the neck radius $c(\chi)$ and the dissipation tensor $\gamma(\chi)$.

APPENDIX B: 3QS SHAPE FAMILY

The three-quadratic-surface shape family introduced by Nix [30] consists of axially symmetric shapes for which the square of the local radial distance $\rho(z)$ to the surface is given by three smoothly joined quadratic surfaces,

$$\rho^2(z) = \begin{cases} a_1^2 - (a_1^2/c_1^2)(z - \ell_1)^2, & \ell_1 - c_1 \leqslant z \leqslant z_1, \\ a_3^2 - (a_3^2/c_3^2)(z - \ell_3)^2, & z_1 \leqslant z \leqslant z_2, \quad \text{(B1)} \\ a_2^2 - (a_2^2/c_2^2)(z - \ell_2)^2, & z_2 \leqslant z \leqslant \ell_2 + c_2. \end{cases}$$

Thus nine numbers are required to specify the nuclear surface. Two of these are eliminated due to the continuity of $\rho(z)$ and its derivative at z_1 and z_2, and the length parameter $u = [\frac{1}{2}(a_1^2 + a_2^2)]^{1/2}$ governs the overall scale. The remaining six numbers are then determined by six dimensionless shape parameters $\{q_\nu\}$,

$$\sigma_1 = \frac{\ell_2 - \ell_1}{u}, \quad \sigma_2 = \frac{a_3^2}{c_3^2}, \quad \sigma_3 = \frac{1}{2}\left(\frac{a_1^2}{c_1^2} + \frac{a_2^2}{c_2^2}\right), \quad \text{(B2)}$$

$$\alpha_1 = \frac{\ell_1 + \ell_2}{u}, \quad \alpha_2 = \frac{a_1^2 - a_2^2}{u^2}, \quad \alpha_3 = \frac{a_1^2}{c_1^2} - \frac{a_2^2}{c_2^2}. \quad \text{(B3)}$$

Furthermore, if the shapes are required to have a given center of mass, then the parameter α_1 is determined once the other five have been specified. All the shapes in the $IJKLM$ lattice have their center of mass at the origin, which effectively reduces the six-dimensional $\{q_\nu\}$ space to the five-dimensional shape space covered by the $IJKLM$ lattice.

For the evaluation of the dissipation tensor $\gamma_{\mu\nu}$, we need the derivatives $\partial \rho^2/\partial q_\nu$ as well as $\partial \rho^2/\partial z$ which, though somewhat involved, can be expressed analytically [29].

The 3QS family includes shapes for which one of the three segments covers only a negligible z interval. The contribution from such a segment to the dissipation rate is then also negligible and, as a result, so are the associated elements of the dissipation tensor. These singularities are numerically inconvenient and must be addressed.

[1] J. Randrup and P. Möller, Phys. Rev. Lett. **106**, 132503 (2011).

[2] P. Möller, A. J. Sierk, T. Ichikawa, A. Iwamoto, R. Bengtsson, H. Uhrenholt, and S. Åberg, Phys. Rev. C **79**, 064304 (2009).

[3] L. Meitner and O. R. Frisch, Nature (London) **143**, 239 (1939).

[4] N. Bohr, Nature (London) **143**, 330 (1939).

[5] N. Bohr and J. A. Wheeler, Phys. Rev. **56**, 426 (1939).

[6] A. J. Sierk and J. R. Nix, Phys. Rev. C **21**, 982 (1980).

[7] J. Blocki, Y. Boneh, J. R. Nix, J. Randrup, M. Robel, A. J. Sierk, and W. J. Swiatecki, Ann. Phys. **113**, 330 (1978).

[8] J. Randrup and W. J. Swiatecki, Ann. Phys. **125**, 193 (1980).

[9] K. T. R. Davies, A. J. Sierk, and J. R. Nix, Phys. Rev. C **13**, 2385 (1976).

[10] A. J. Sierk, S. E. Koonin, and J. R. Nix, Phys. Rev. C **17**, 646 (1978).

[11] H. A. Kramers, Physica **7**, 284 (1940).

[12] P. Grange, H. C. Pauli, and H. A. Weidenmüller, Phys. Lett. B **88**, 9 (1979).

[13] H. Hofmann and J. R. Nix, Phys. Lett. B **122**, 117 (1983).

[14] P. Grangé, L. Jun-Qing, and H. A. Weidenmüller, Phys. Rev. C **27**, 2063 (1983).

[15] J. R. Nix, A. J. Sierk, H. Hofmann, F. Scheuter, and D. Vautherin, Nucl. Phys. A **424**, 239 (1984).

[16] F. Scheuter, C. Grégroire, H. Hofmann, and J. R. Nix, Phys. Lett. B **149**, 303 (1984).

[17] Y. Abe, S. Ayik, P.-G. Reinhard, and E. Suraud, Phys. Rep. **275**, 49 (1996).

[18] P. Fröbrich and I. I. Gontchar, Phys. Rep. **292**, 131 (1998).

[19] G. Chaudhuri and S. Pal, Phys. Rev. C **63**, 064603 (2001).

[20] A. V. Karpov, P. N. Nadtochy, D. V. Vanin, and G. D. Adeev, Phys. Rev. C **63**, 054610 (2001).

[21] P. N. Nadtochy, A. Kelić, and K.-H. Schmidt, Phys. Rev. C **75**, 064614 (2007).

[22] P. Möller, D. G. Madland, A. J. Sierk, and A. Iwamoto, Nature (London) **409**, 785 (2000).

[23] A. Einstein, Ann. Phys. **17**, 549 (1905).

[24] J. Randrup, Nucl. Phys. A **307**, 319 (1978); **327**, 490 (1979).

[25] W. U. Schröder, J. R. Birkelund, J. R. Huizenga, W. W. Wilcke, and J. Randrup, Phys. Rev. Lett. **44**, 308 (1980).

[26] N. Metropolis, A. W. Rosenbluth, M. N. Rosenbluth, A. H. Teller, and E. Teller, J. Chem. Phys. **26**, 1087 (1953).

[27] M. B. Chadwick *et al.*, Nucl. Data Sheets **107**, 2931 (2006).

[28] K.-H. Schmidt *et al.*, Nucl. Phys. A **665**, 221 (2000).

[29] J. R. Nix, Report No. UCRL-17958, preprint of Ref. [30] (unpublished).

[30] J. R. Nix, Nucl. Phys. A **130**, 241 (1969).

[31] S. E. Koonin and J. Randrup, Nucl. Phys. A **289**, 475 (1977).

[32] P. Möller, Nucl. Phys. A **192**, 529 (1972).

[33] M. Bolsterli, E. O. Fiset, J. R. Nix, and J. L. Norton, Phys. Rev. C **5**, 1050 (1972).

[34] J. Benlliure, A. Grewe, M. de Jong, K.-H. Schmidt, and S. Zhdanov, Nucl. Phys. A **628**, 458 (1998).

[35] K.-H. Schmidt, J. Benlliure, and A. R. Junghans, Nucl. Phys. A **693**, 169 (2001).

[36] P. Möller, A. J. Sierk, and A. Iwamoto, Phys. Rev. Lett. **92**, 072501 (2004).

[37] W. D. Myers, *Droplet Model of Atomic Nuclei*, (IFI/Plenum, New York, 1977).

[38] P. Möller, J. R. Nix, and W. J. Swiatecki, Nucl. Phys. A **492**, 349 (1989).

[39] P. Möller and J. R. Nix, J. Phys. G **20**, 1681 (1994).

[40] W. D. Myers and W. J. Swiatecki, Nucl. Phys. A **601**, 141 (1996).

[41] W. D. Myers and W. J. Swiatecki, Nucl. Phys. A **612**, 249 (1997).

[42] P. Möller, J. R. Nix, W. D. Myers, and W. J. Swiatecki, At. Data Nucl. Data Tables **59**, 185 (1995).

[43] S. Goriely, M. Samyn, P.-H. Heenen, J. M. Pearson, and F. Tondeur, Phys. Rev. C **66**, 024326 (2002).

[44] A. V. Ignatyuk, K. K. Istekov, and G. N. Smirenkin, Sov. J. Nucl. Phys. **21**, 255 (1975).

[45] P. Fong, Phys. Rev. **102**, 434 (1956).

[46] B. D. Wilkins, E. P. Steinberg, and R. R. Chasman, Phys. Rev. C **14**, 1832 (1976).

[47] A. N. Andreyev *et al.*, Phys. Rev. Lett. **105**, 252502 (2010).